

INTRODUCTION TO EXTRAGALACTIC SOURCES OF VERY HIGH-ENERGY PHOTONS

C. PFROMMER

Heidelberg Institute for Theoretical Studies, Schloss-Wolfsbrunnengasse 35, 69118 Heidelberg, Germany

The launch of the *Fermi* gamma-ray space telescope and the imaging air Cerenkov telescopes H.E.S.S., MAGIC, and VERITAS have substantially transformed our knowledge of gamma-ray sources in the last decade. The extragalactic gamma-ray sky is teeming with blazars, which are active galactic nuclei whose jet is directed at us. Additionally, there are radio galaxies, starburst and spiral galaxies, and gamma-ray bursts, albeit with smaller numbers. Galaxy clusters have not yet been observed in gamma rays. Here, I will introduce the different gamma-ray emission processes and review what they may tell us about these objects and the underlying acceleration mechanisms. Beyond the study of these fascinating objects, TeV gamma rays from blazars probe the integrated star formation history of the universe. Studies of TeV blazar spectra may provide us with insights into intergalactic magnetic fields or alternatively, may lead us to infer the existence of a novel mechanism that heats the intergalactic medium at late times (for redshifts $z < 3$) and impacts the Lyman- α forest and late-time structure formation. The TeV gamma-ray emission may also allow us to probe fundamental physics such as the structure of space time.

1 Introduction

Gamma rays cannot penetrate the Earth's atmosphere to the ground. To directly detect them, we have to go to space, where the Large Area Telescope onboard *Fermi* is currently surveying the entire sky at energies ranging from around 100 MeV to 100 GeV. The upper energy limit is determined by the finite size of the detector, which uses the pair conversion technique to detect gamma rays. However, for a gamma-ray energy above 30 GeV, it is feasible to detect the flash of Cerenkov light that is emitted in the electromagnetic cascade initiated by the gamma ray penetrating the Earth's upper atmosphere. This allows to reconstruct the energy and arrival direction of the original gamma ray and opens a second window to the gamma-ray sky that is employed by the imaging air Cerenkov telescope collaborations H.E.S.S., MAGIC, and VERITAS. Those have to conduct pointed observations of interesting targets. While this allows deeper observations on single objects with better angular resolution, it complicates the characterization of the selection function for population studies. What are the main questions that we can address by observationally probing the extragalactic gamma-ray sky?

- Which objects can we see? Clearly, we can do astronomy in the gamma-ray band and characterize and classify the detected objects into populations. Using multi-frequency constraints, we can then identify the objects with known counterparts at other electromagnetic wavelengths. Gamma-ray emitting objects are active galactic nuclei (blazars, radio galaxies), starburst and spiral galaxies, and gamma-ray bursts.
- What underlying physics can we probe? In practice, gamma-ray emission probes the most extreme physics laboratories of the cosmos. This allows us to assess questions about

the mechanism of particle acceleration and magnetic field amplification, and to study plasma physical processes at conditions that are quite different from those achievable in our laboratories on Earth (e.g., collisionless plasmas, extreme Lorentz factors).

- What fundamental physics can we hope to learn? (1) TeV photons produce electron-positrons pairs upon annihilating with soft photons in the extragalactic background light. This process enables us to probe the integrated star formation history of the universe. (2) It also may provide us with insights into intergalactic magnetic fields (which could be of primordial origin). (3) If the kinetic pair energy can be efficiently dissipated, this may even provide the dominant energy source to the intergalactic medium at late times (for redshifts $z < 3$) and hence impact the intergalactic medium, the Lyman- α forest and late-time structure formation. (4) Extreme variability at the highest gamma-ray energies may enable us to probe the structure of space time. (5) The gamma-ray energies are well adapted to the weak energy scale, which coincides with the dark matter particle masses in the most popular models since those weakly interacting massive particles would naturally account for the observed relic density if they had thermally decoupled in the early universe. Hence, studies of the physics associated with gamma rays can provide essential clues for our understanding of structure formation, cosmology, and particle physics.

After introducing the different gamma-ray emission processes, I will discuss each object class and the physics that this allows us to probe. This is meant to be a pedagogical introduction rather than a comprehensive review for which the reader is referred to Rieger *et al.* (2013).

2 Gamma-ray emission processes induced by cosmic rays

Gamma rays carry complementary information to cosmic rays (CRs) and unlike the latter, point back to their origin (except for the ultra-high-energy CRs that perhaps are also little deflected by intervening magnetic fields). We distinguish *hadronic processes* (as a result of CR proton- or ion-initiated interactions) and *leptonic processes* due to relativistic electrons or positrons. At the heart of all of these emission processes are the acceleration mechanisms that produce a (non-thermal) population of relativistic protons or electrons in first place. Gamma-ray observations can thus give us some constraints on the underlying type of acceleration.

hadronic processes:

- pion decay:

$$p + p(\text{ion}) \rightarrow \begin{cases} \pi^0 & \rightarrow \gamma\gamma \\ \pi^\pm & \rightarrow e^\pm + \nu_\mu + \bar{\nu}_\mu + \overset{(-)}{\nu}_e \end{cases}$$

- photo-meson production:

$$p(\text{ion}) + \gamma \rightarrow \begin{cases} \pi^0 & \rightarrow \gamma\gamma \\ \pi^\pm & \rightarrow e^\pm + \nu_\mu + \bar{\nu}_\mu + \overset{(-)}{\nu}_e \end{cases}$$

- Bethe-Heitler pair production:

$$p(\text{ion}) + \gamma \rightarrow p(\text{ion}) + e^+ + e^-$$

leptonic processes:

- inverse Compton:

$$e^* + \gamma \rightarrow e + \gamma^*$$

- synchrotron radiation:

$$e^*(p^*) + B \rightarrow e(p) + B + \gamma^*$$

- bremsstrahlung:

$$e^* + p(\text{ion}) \rightarrow e + p(\text{ion}) + \gamma^*$$

The hadronic p-p reaction proceeds if the center-of-momentum energy exceeds the kinetic energy threshold of the pion rest mass (or more precisely the Δ resonance through which this reaction proceeds). The latter two *hadronic processes* require that the gamma-ray energy in the rest system of the proton (ion) exceeds the rest mass of the pion or twice that of the electron, respectively. This can either be achieved by a CR interacting with a soft photon that is Lorentz

boosted to the CR's rest frame or by an energetic gamma ray. The latter could result from either of the *leptonic processes* (shown on the right; a star denotes here an energetic particle).

Inverse Compton emission and synchrotron emission are very similar processes since both describe the interaction of an energetic lepton with a photon. This photon can either be provided by an astrophysical radiation field or is a virtual photon that mediates the electromagnetic interaction of the electron with the magnetic field B . Because the synchrotron emissivity of a particle with mass m scales with the Thompson cross section, $\sigma_T \propto m^{-2}$, protons have to be more energetic by a factor of $(m_p/m_e)^2$ to produce an emission that is comparable to that of electrons. Finally, (non-)thermal bremsstrahlung emission is caused by the acceleration of a (non-)thermal electron in the Coulomb field of an ion. The gamma-ray spectra resulting from these non-thermal processes are typically power-law spectra that reflect the parent CR (electron or proton) power-law spectra and are convolved with the respective emission spectrum of an individual particle. Changing to a dimensionless integration variable determines the relation between spectral indices of the CR and gamma-ray emission spectra.

3 Active galactic nuclei

Active galactic nuclei (AGN) can launch relativistic jets that are powered by accretion onto a central nucleus, presumably a supermassive black hole. The widely accepted AGN standard paradigm provides a unified picture of their emission properties, which depend on the orientation of the AGN relative to the line of sight (Urry *et al.* 1995). There exist two main classes of AGNs that differ in their accretion mode and in the physical processes that dominate the emission.

- *Thermal/disk-dominated AGNs.* Infalling matter assembles in a thin disk and radiates thermal emission with a range of temperatures. The distributed black-body emission is then Comptonized by a hot corona above the disk that produces power-law X-ray emission, which is a measure of the accretion power of the central object. This class of objects are called QSOs or Seyfert galaxies and make up about 90% of AGNs. They preferentially emit in the optical or X-rays and do not show significant nuclear radio emission. None of these sources have so far been unambiguously detected by *Fermi* or imaging atmospheric Cherenkov telescopes because the Comptonizing electron population is not highly relativistic and emits isotropically, i.e. there is no relativistic beaming effect that boosts the emission.
- *Non-thermal/jet-dominated AGNs.* Highly energetic electrons that have been accelerated in the relativistic jet interact with the jet magnetic field and emit synchrotron photons that range from the radio to X-ray. The same population of electrons can also Compton up-scatter any seed photon population either provided by the synchrotron emission itself (*synchrotron self-Compton scenario*) or from some other external radiation field such as ultraviolet (UV) radiation from the accretion disk or the infrared (IR) radiation from the surrounding torus (*external Compton scenario*). Hence the spectral energy distribution (SED) of these objects shows two distinct peaks. Alternatively, sufficiently energetic *proton synchrotron* photons can be converted into a pion in the Coulomb field of a proton. The neutral pion decays into gamma rays that trigger an electromagnetic cascade, which produces a spectrum of gamma rays (*proton-induced cascades*). The luminosity of all these non-thermal emission components probes the jet power of these objects. Observationally, this leads to the class of radio-loud AGNs which can furthermore be subdivided into blazars (with the line of sight intersecting the jet opening angle) and non-aligned non-thermal dominated AGNs.

Blazars can further be subdivided into two main subclasses depending upon their optical spectral properties: flat spectrum radio quasars (FSRQ) and BL Lacs. FSRQs, defined by broad optical emission lines, have SEDs that peak at energies below 1 eV, implying a maximum particle energy

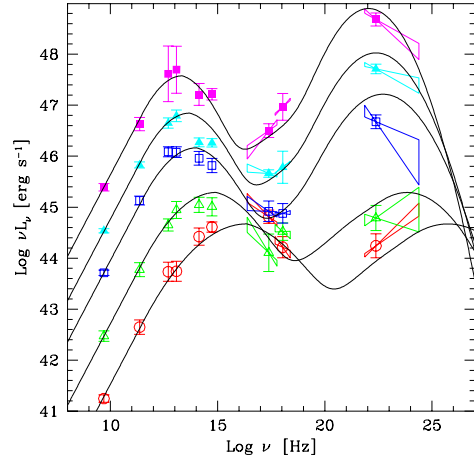


Figure 1: *Left.* Artist’s impression of a super-massive black hole that launches relativistic jets and electromagnetic radiation out to cosmological distances. Blazars are systems where the jet opening angle contains our line of sight, i.e. the jet “points” at us (credit ESA/NASA/AVO/Padovani). *Right.* Sequence of characteristic blazar SEDs as a function of source luminosity from FSRQ (top curve) to HSP objects (bottom curve, from Donato *et al.* 2001).

within the jet and limiting the inverse-Compton scattered photons mostly to the soft gamma-ray band. It is presumably for this reason that no continuous TeV component has been detected in an FSRQ (while their flare emission can sometimes reach TeV energies).

In contrast, BL Lacs or Blazars of the BL Lac type (Massaro *et al.* 2009) can be copious TeV emitters. These are very compact radio sources and have a broadband SED similar to that of strong lined blazars but lack the broad emission lines that define those. Depending upon the peak energy in the synchrotron spectrum, which approximately reflects the maximum particle energy within the jet, they are classified as low-, intermediate-, or high-synchrotron peaked BL Lacs, respectively called LSP, ISP, and HSP. While LSPs peak in the far-IR or IR band, they exhibit a flat or inverted X-ray spectrum due to the dominance of the inverse-Compton component (see Fig. 1). The synchrotron component of ISPs peaks in the optical, which moves their inverse-Compton peak into the gamma-ray band of *Fermi*. HSPs are much more powerful particle accelerators, with the synchrotron peak reaching into the UV or, in some cases, the soft X-ray bands. The inverse-Compton peak can then reach TeV energies.

Hard *Fermi* blazars (defined by a rising energy spectrum, $E^2 dN/dE$, in the *Fermi* band, i.e., HSPs and some ISPs) have a redshift distribution that is peaked at low redshifts extending only up to $z = 0.7$. This is most likely entirely a flux selection effect; hard blazars are intrinsically less luminous than LSPs and FSRQs, with an observed isotropic-equivalent luminosity range of $10^{44} - 2 \times 10^{46}$ erg s $^{-1}$, with the highest redshift hard *Fermi* blazars also being among the most luminous objects. There are plausible explanations why hard *Fermi* blazars should be intrinsically less luminous than FSRQs. Ghisellini *et al.* (2009) have argued that the physical distinction between FSRQs and hard blazars has its origin in the different accretion regimes of the two classes of objects. Using the gamma-ray luminosity as a proxy for the bolometric luminosity, the boundary between the two subclasses of blazars can be associated with the accretion rate threshold (nearly 1% of the Eddington rate) separating optically thick accretion disks with nearly Eddington accretion rates from radiatively inefficient accretion flows. The spectral separation in hard (BL Lacs) and soft (FSRQs) objects then results from the different radiative cooling suffered by the relativistic electrons in jets propagating into different surrounding media (Ghisellini *et al.* 2009). Hence in this model, hard *Fermi* blazars cannot reach higher luminosities than approximately 2×10^{46} erg s $^{-1}$ since they are limited by the nature of inefficient accretion flows that power these jets and by the maximum black hole mass, $\sim 10^{10} M_{\odot}$.

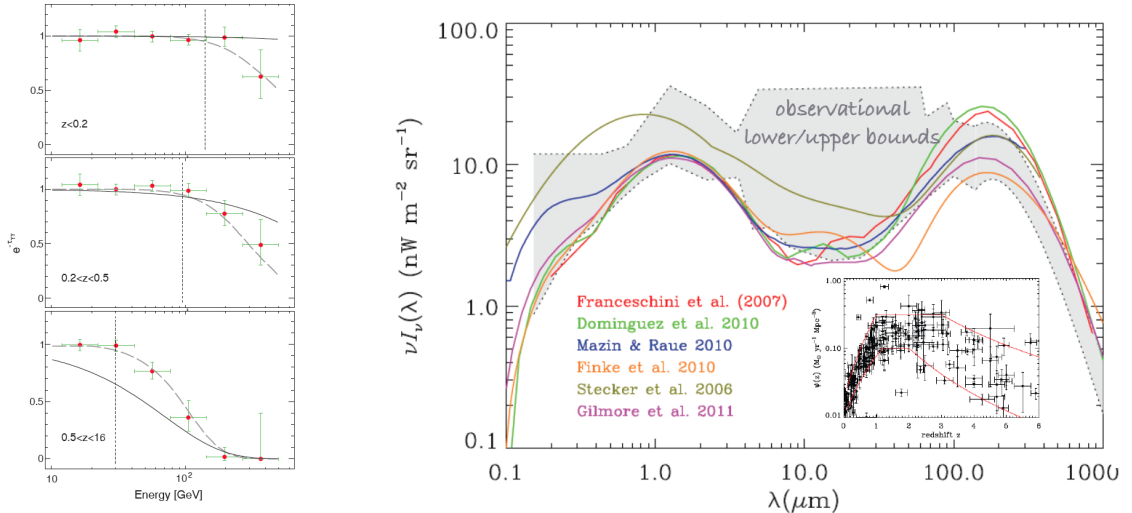


Figure 2: *Left.* Stacked spectra of BL Lac objects show an absorption feature that moves to lower energies for increasing redshift (data points, from top to bottom). This confirms that gamma rays are attenuated by annihilating and pair producing on the EBL (dashed curve) and rules out models where all blazars have an intrinsic exponential cutoff and follow the blazar sequence (thin solid, from M. Ackermann *et al.* 2012). *Right.* Models of the EBL are compared to observational limits on the EBL. The inset shows a compilation of the cosmic star formation rate as inferred from UV, H α , mid-IR, submillimeter, radio, and Ly α observations while excluding lower limits (from Dwek & Krennrich 2012).

Despite the tremendous progress in our understanding of properties of the various populations, there are many open questions, including the jet energetics, the mechanisms responsible for jet formation and collimation, the plasma composition (leptonic vs. hadronic), the jet geometry (1-zone vs. spine-layer), or the specific acceleration mechanisms of the jet plasma. Particularly puzzling is the reason for the observed variability of the gamma-ray emission of blazars, which is considerably smaller than the light crossing time of the Schwarzschild horizon in the most extreme cases. TeV “flares” may sign instabilities in the accretion of matter onto the central supermassive black hole or in the jet.

4 The impact of TeV blazars on cosmology and structure formation

The light emitted by galaxies and accreting compact objects throughout the history of the universe is encoded in the intensity of the *extragalactic background light* (EBL). Hence it provides an important integral constraint on the star and quasar formation history in the hierarchical model of galaxy assembly. Direct measurements of the EBL are limited by galactic and other foreground emissions. Instead one can infer it indirectly because the universe is opaque to TeV gamma rays, which annihilate and pair produce on the EBL. This implies an absorption feature (the “gamma-ray horizon”) in the spectra of gamma-ray blazars. Stacking the spectra of 150 significantly detected BL Lac blazars ($0.03 < z < 1.6$), the *Fermi* Collaboration showed that the stacked spectrum is unabsorbed for $E < 25$ GeV. In agreement with the expectation, there is an absorption feature that moves to lower gamma-ray energies for higher source redshifts (propagation distances) due to attenuation of gamma rays by the EBL at optical to UV frequencies (Ackermann *et al.* 2012, see Fig. 2).

The ultra-relativistic pairs of electrons and positrons resulting from TeV photon annihilation on the EBL are commonly assumed to lose energy primarily through inverse Compton scattering with photons of the cosmic microwave background, cascading the original TeV emission a factor of $\sim 10^3$ down to GeV energies. However, the expected cascaded GeV emission is not seen in the individual spectra of those blazars (Neronov & Vovk 2010). As a putative solution to this problem, *intergalactic magnetic fields* have been hypothesized, which would deflect the pairs out

of our line-of-sight to these blazars, diluting the point-source flux into a lower surface brightness “pair halo”. A stronger magnetic field implies more deflection and dilution of the GeV point source flux. In this picture, a non-detection of GeV gamma rays suggests a limit on intergalactic magnetic fields of $B \gtrsim (10^{-17} - 10^{-15}) \mu\text{G}$ for a magnetic coherence length of 1 Mpc, where the range covers uncertainties about the time delay of the cascade photons (Taylor *et al.* 2011). Since most of the volume of the universe (and hence a random sight line) is dominated by voids, magnetic fields of these strengths may imply a primordial origin and allow one of these rare glimpses into the early universe.

However, it has been shown recently that there is an even more efficient mechanism that competes with this cascading process. The ultra-relativistic pairs, originating from TeV photon annihilation on the EBL, are propagating through the intergalactic medium, which can be viewed as two counter-propagating beams that are subject to plasma instabilities. The linear growth rate of the so-called “oblique instability” is larger than the inverse Compton cooling rate of the pairs. If this dominance of the instability growth rate carries over to the regime of non-linear saturation, this implies a transfer of free kinetic energy of the pairs to the unstable electromagnetic modes in the background plasma, which should eventually be dissipated, heating the intergalactic medium (Broderick *et al.* 2012, Schlickeiser *et al.* 2012). Typically, ~ 300 yr after the onset of TeV emission, the pair beam density has grown sufficiently for plasma beam instabilities to dominate its evolution, randomize the beam, and potentially suppress the inverse-Compton signal upon which the limits on the intergalactic magnetic fields are based (rendering these limits dubious). In this picture, there are two means to avoid the consequences of plasma beam instabilities during the growth of the pair beam by (1) the sudden appearance of a TeV-bright blazar or intrinsically transient sources (e.g., gamma-ray bursts) or (2) for particularly dim sources, $L \lesssim 10^{42} \text{ erg s}^{-1}$, for which the pair beam density is too small to support collective plasma behaviour. However, for all luminous TeV blazars detected to date, the presence of these plasma beam instabilities appears unavoidable and suggests the existence of a novel heating mechanism, coined *blazar heating*. It produces an inverted temperature-density relation of the intergalactic medium (Chang *et al.* 2012) that is in agreement with observations of the Lyman- α forest (Puchwein *et al.* 2012). This also suggests that *blazar heating* can potentially explain the paucity of dwarf galaxies in galactic halos and voids, and the bimodality of central gas entropy values in galaxy clusters (Pfrommer *et al.* 2012). Detailed comparisons of predictions of blazar heating with *Fermi* observation of blazar statistics (redshift and $\log \mathcal{N}$ - $\log S$ distribution) as well as the isotropic and anisotropy gamma-ray backgrounds have been very successful and supportive of this model (Broderick *et al.* 2013).

5 Blazar and gamma-ray burst variability probes the structure of space time

Blazar variability shows a complex multi-wavelength behaviour that challenges simple emission models. The H.E.S.S. observation of a giant flare (more than two orders of magnitudes) of PKS 2155-304 shows a variability timescale $\Delta t_{\text{var}} \sim (2 - 3) \text{ min} \sim 0.02 R_s/c$, where R_s/c is the light crossing time of the Schwarzschild horizon (Aharonian *et al.* 2008). Causality requires $R < c\Delta t_{\text{var}}\gamma$ and implies a very small emission region and bulk motion with a Lorentz factor $\gamma > 50$ (Begelmann *et al.* 2008).

Independent of the emission mechanism, the observed variability can also be used to probe the structure of space time and to constrain theories of Quantum Gravity, some of which predict space-time to be “foamy” or discrete at the Planck scale $l_P = \hbar/(m_P c)$, where the Planck mass is $m_P = \sqrt{\hbar c/G}$. Preserving the $O(3)$ subgroup of $SO(3, 1)$, we can parametrize the modified dispersion relation for photons, $c^2 \mathbf{p}^2 = E^2(1 + \xi E/E_{\text{QG}} + \eta E^2/E_{\text{QG}}^2 + \dots)$, where it is usually assumed that $E_{\text{QG}} \sim m_P c^2 \sim 10^{19} \text{ GeV}$ and $\xi = \pm 1$ is a sign ambiguity that is fixed in a given dynamical framework. Assuming that the Hamiltonian equations of motion, $\dot{x}_i = \partial H/\partial p_i$, are still valid, this yields $v = \partial E/\partial p = c(1 - \xi E/E_{\text{QG}} + \dots)$. In other words, we obtain

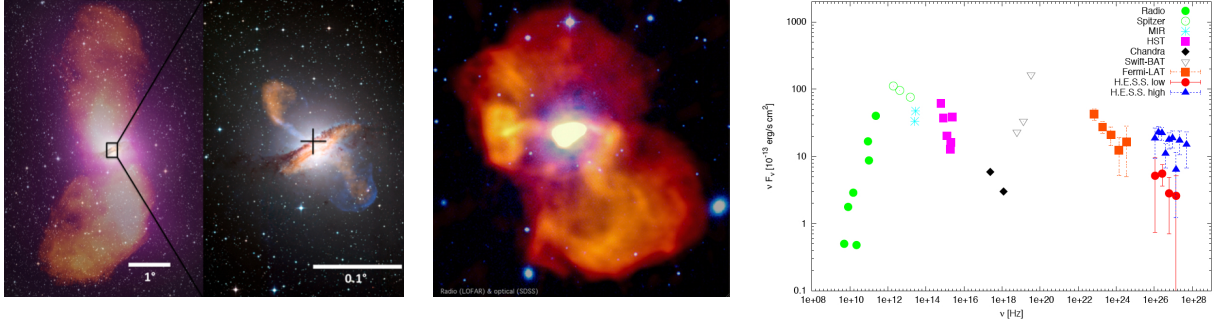


Figure 3: Nearby radio galaxies are emitting in gamma rays. *Fermi* and H.E.S.S. detected gamma-ray emission from Cen A (left, radio data in orange are overlaid on *Fermi* data in purple, credit NASA/DOE/*Fermi* LAT) and M87 (middle, 140 MHz radio data from LOFAR/de Gasperin *et al.* 2012). Right. Multi-frequency spectrum of M87 indicating the low- (red) and high-flux state (blue) at TeV energies (from Rieger & Aharonian 2012).

an energy-dependent time delay $\Delta t = \xi(E/E_{\text{QG}})(L/c) = 10 \text{ ms} (\text{GeV}/E_{\text{QG}})(1 \text{ Gpc}/c)$, where L is the path length of the photon. That is, we can test this by studying propagation of high energy gamma-ray pulses of different energies from cosmological distances (Amelino-Camelia *et al.* 1998).

That test was done with the *Fermi* detection of the early arrival time of the 31 GeV photon of the short gamma-ray burst GRB 090510, implying a conservative bound of $E_{\text{QG}} > 1.2 \times 10^{19} \text{ GeV}$ (Abdo *et al.* 2009a). The giant flare of PKS 2155-304 observed by H.E.S.S. shows no observable time delay between low- and high-energy photons, thereby implying a bound $E_{\text{QG}} > 2.1 \times 10^{18} \text{ GeV}$ (Abramowski *et al.* 2011). This starts to constrain an energy-dependent violation of Lorentz invariance (i.e., an energy-dependent speed of light), which is predicted in various models of Quantum Gravity. However, all these analyses make the strong assumption that there is no intrinsic gamma-ray dispersion in the source and that the gamma-ray pulses at different energies are emitted at the same time. To improve upon these constraints, we need a better understanding of the sources and emission mechanisms.

6 Radio galaxies and the cluster “cooling flow problem”

Some nearby radio galaxies also emit gamma rays, which may be partly related to the nucleus, the jet, the radio lobes, or CR interactions with the surrounding plasma (see Fig. 3). The closest radio galaxy Centaurus A is at a distance of 3.7 Mpc, often considered as an “AGN under the microscope”. *Fermi* observes GeV emission from the giant radio lobes and the core while H.E.S.S. detected TeV emission from the nucleus/inner jet (Abdo *et al.* 2010, Aharonian *et al.* 2009). This triggered ideas that the giant lobes are the sites of high-energy particle acceleration and production of ultra-high-energy cosmic rays (Hardcastle *et al.* 2009).

At the end of the momentum-driven phase, relativistic jet particles inflate radio-emitting lobes and do pressure-volume work on the ambient intra-group and -cluster medium. According to the current paradigm, the buoyantly rising lobes either do mechanical work on the surroundings (which gets dissipated through shocks or a turbulent cascade) or they release CRs into the intracluster medium. Those stream at the Alfvén velocity with respect to the plasma rest frame and heat the surrounding thermal plasma (Loewenstein *et al.* 1991). This “AGN feedback” balances radiative cooling and solves the cluster “cooling flow problem” at low redshifts, $z \lesssim 1$ (McNamara & Nulsen 2012). What can gamma-ray observations add to this picture?

Fermi and H.E.S.S. discovered gamma-ray emission from the radio galaxy M87 (Abdo *et al.* 2009b, Abramowski *et al.* 2012), the central galaxy of the Virgo cluster, our closest galaxy cluster at a distance of 17 Mpc. While the TeV emission in the high state is likely connected to the emission from the nucleus/jet, there is the possibility that the low emission state traces pion-decay gamma rays from the Virgo cool-core region as implied by the spectral similarity

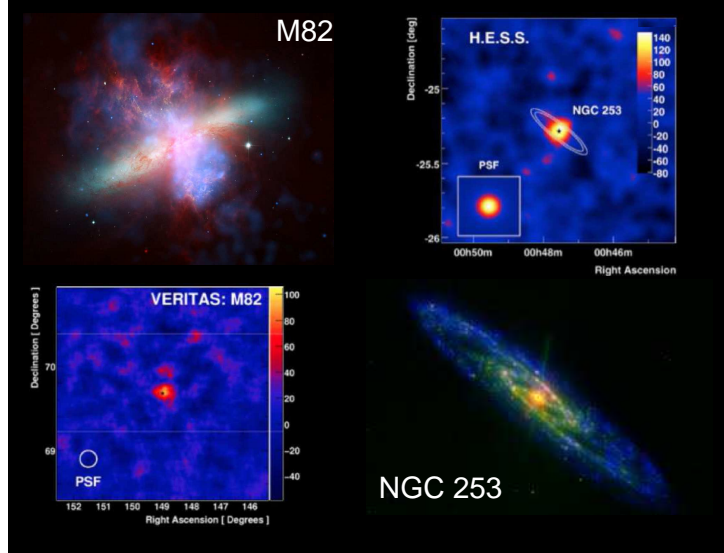


Figure 4: The nearby starburst galaxies M82 (Acciari *et al.* 2009) and NGC 253 (Acero *et al.* 2009) emit TeV gamma rays. We contrast gamma-ray significance maps to optical images of these galaxies.

to LOFAR radio data (see Fig. 3). In this picture, the gamma-ray emission can be used to normalize the CR-induced heating rate, which balances that of radiative cooling *on average* at each radius, thereby suggesting a solution to the “cooling flow problem” in the Virgo cluster (Pfrommer 2013). This model would predict the gamma-ray emission in the low state to be steady and slightly extended, which is testable with current observations.

7 Starburst and spiral galaxies

M82 and NGC 253 are TeV gamma-ray emitting starburst galaxies (Acciari *et al.* 2009, Acero *et al.* 2009), both at a distance of ~ 3 Mpc (see Fig. 4). *Fermi* confirmed the gamma-ray emission in those objects and increased the sample of starburst galaxies by two more objects (NGC 4945, NGC 1068) although those are composite starburst/Seyfert 2 systems, which makes it challenging to disentangle the pure starburst component (Lenain *et al.* 2010). Their star formation rate (in a compact region) is larger than that of the Milky Way. In the emerging picture, supernova remnants, associated with star formation regions, can energize CR protons through diffusive shock acceleration. Hadronic interactions of those CR protons with the ambient dense gas produce pion-decay gamma rays. In the starburst region, there is dense interstellar gas, with $\langle n \rangle \sim 250 \text{ cm}^{-3}$, which yields a hadronic interaction time that is of order the diffusive escape time, $t_{pp} \sim t_{esc}$. Hence we are approaching the calorimetric limit.

The large magnetic field strengths and high densities should also give rise to efficient leptonic emission. In fact, the tight far infrared (FIR)–radio correlation implies universal conversion of the star formation rate to the CR- and the synchrotron luminosities. Provided the picture of gamma-ray emission is correct, this also would imply a FIR–gamma-ray correlation. The local four spiral galaxies (Milky Way, SMC, LMC, M31) show indeed gamma-ray luminosities, which fall on the locus of the FIR–gamma-ray correlation defined by the starburst galaxies. However, to fully establish this picture, the AGN contribution to the observed gamma-ray emission of starburst galaxies needs to be carefully quantified. Moreover, the possible counterexamples to this relation, i.e., upper limits on the gamma-ray emission of some galaxies that fall also within the implied relation (IC342, NGC 6946), need to be understood. While their upper limits are still compatible with the scatter around the relation, tighter limits will either strengthen the tension or lead to a detection, thereby confirming the existence of a FIR–gamma-ray correlation.

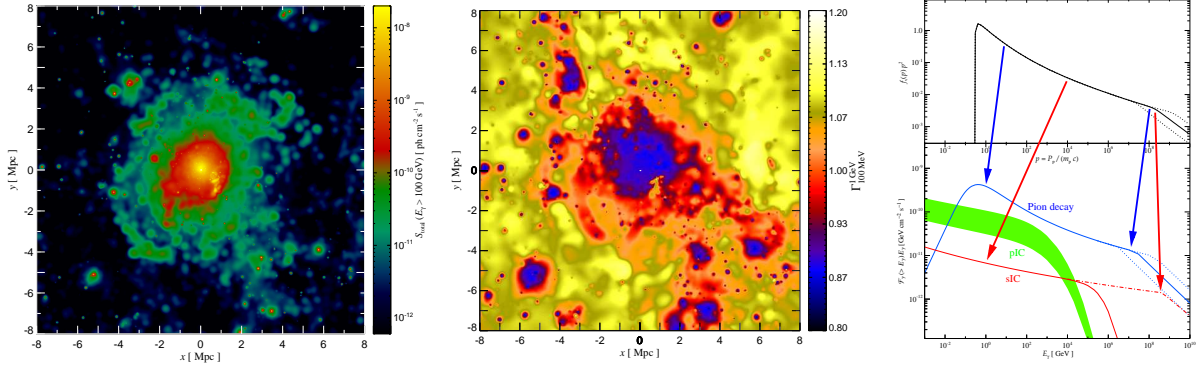


Figure 5: Expected gamma-ray emission in a cosmological hydrodynamical simulation of a galaxy cluster. The surface brightness emission (*left*) and spectral index map, $\Gamma_{100 \text{ MeV}}^{1 \text{ GeV}}$, (*middle*) is dominated in the center by pion decay and outside the virial radius (of 2.4 Mpc) by primary inverse Compton (pIC) emission from shock-accelerated relativistic electrons. The total CR proton spectrum shows a universal shape across clusters (*top right*) that is inherited by the pion decay and secondary IC emission following hadronic p-p interactions (*bottom right*). The pIC emission only has a small contribution to the total emission for $E > 30 \text{ MeV}$ (from Pinzke & Pfrommer 2010).

8 Galaxy clusters

Despite many efforts in the recent years, no cluster-wide gamma-ray emission has been detected so far (Ackermann *et al.* 2010, 2013). The observed radio halo and relic emission on cluster scales (1-3 Mpc) proves the existence of CR electrons and magnetic fields that permeate the cluster volumes and suggests that clusters also emit diffuse gamma rays. Cosmological hydrodynamical simulations of galaxy cluster with self-consistent CR physics show that the normalized CR spectrum has a universal concave shape across clusters (Pinzke & Pfrommer 2010). During the hierarchical assembly, every fluid element experienced on average the same history of shock strengths, which is responsible for shaping the CR spectrum. As a result, the gamma-ray signal is expected to be dominated by pion decay, but other possibilities exist, such as inverse Compton emission from electrons that have been accelerated at structure formation shock waves (see Fig. 5).

Non-observations of gamma rays from the Perseus and Coma clusters constrain the CR-to-thermal pressure to $P_{\text{CR}}/P_{\text{th}} < 1.7\%$ in those clusters (Aleksic *et al.* 2012, Arlen *et al.* 2012). This immediately implies that hydrostatic cluster masses are not significantly biased by CRs—an important result if cluster populations are to be used for determining cosmological parameters. A comparison to hydrodynamical cluster simulations constrains the maximum acceleration efficiency at formation shock on average to $< 50\%$. Provided the (*high-frequency*) radio halo emission is produced by secondary electrons from CRp-p interactions, this allows us to place limits on the central cluster magnetic fields of $> (4 - 9) \mu\text{G}$ (Perseus) and $> (2 - 5) \mu\text{G}$ (Coma), which are below the limits obtained from Faraday rotation measure studies (Aleksic *et al.* 2012, Arlen *et al.* 2012). However, these limits on magnetic fields are in conflict with Faraday rotation data for the *low-frequency* radio halo emission in Coma, arguing for a leptonic origin of (at least) the external halo at these frequencies (Brunetti *et al.* 2011).

9 Conclusions

The non-thermal universe revealed by high-energy radiation provides not only deep insights into high-energy astrophysics and plasma processes that are not accessible in our laboratories on Earth but also new probes of fundamental physics, cosmology, and structure formation. With the successful *Fermi* telescope and the imaging air Cerenkov collaborations H.E.S.S., MAGIC, and VERITAS, we are currently entering a fascinating era that is complemented by multi-frequency experiments. As a result of this, there is no shortage of new discoveries and puzzles

to solve. In tackling those, we should not be afraid of employing new ideas and theories, some of which may later need to be refined. In doing so, we should mind the unseen (dark matter, galaxy clusters, ...). What can it teach us? Does it conflict with our previous models of particle acceleration and/or transport? To proceed, a precise and accurate measurement of the isotropic and anisotropic extragalactic gamma-ray background is critical for constraining the luminosity evolution of various populations by their maximally allowed contribution to the respective backgrounds. I will end this introduction by a quote of Louis Pasteur stating that “in the fields of observation chance favors only the prepared mind”!

Acknowledgments

C.P. gratefully acknowledges financial support of the Klaus Tschira Foundation and thanks Chris Hayward for carefully reading the manuscript.

References

- [1] A.A. Abdo *et al.*, *Nature* **462**, 331 (2009a).
- [2] A.A. Abdo *et al.*, *ApJ* **707**, 55 (2009b).
- [3] A.A. Abdo *et al.*, *Science* **328**, 725 (2010).
- [4] A. Abramowski *et al.*, *Astropart.Phys.* **34**, 738 (2011).
- [5] A. Abramowski *et al.*, *ApJ* **746**, 151 (2012).
- [6] V.A. Acciari *et al.* *Nature* **462**, 770 (2009).
- [7] F. Acero *et al.*, *Science* **326**, 1080 (2009).
- [8] M. Ackermann *et al.*, *subm.* (2013) [arXiv:1308.5654](#).
- [9] M. Ackermann *et al.*, *Science* **338**, 1190 (2012).
- [10] M. Ackermann *et al.*, *ApJL* **717**, L71 (2010).
- [11] F. Aharonian *et al.*, *PRL* **101**, 170402 (2008).
- [12] F. Aharonian *et al.*, *ApJ* **695**, L40 (2009).
- [13] J. Aleksic *et al.*, *A&A* **541**, 99 (2010).
- [14] T. Arlen *et al.*, *ApJ* **757**, 123 (2010).
- [15] G. Amelino-Camelia, J. Ellis, N.E. Mavromatos, D.V. Nanopoulos, S. Sarkar, *Nature* **393**, 763 (1998).
- [16] M.C. Begelman, A.C. Fabian, M.J. Rees, *MNRAS* **384**, L19 (2008).
- [17] A.E. Broderick, P. Chang, C. Pfrommer, *ApJ* **752**, 22 (2012).
- [18] A.E. Broderick, C. Pfrommer, E. Puchwein, P. Chang, *subm.* (2013) [arXiv:1308.0340](#).
- [19] G. Brunetti *et al.*, *MNRAS* **426**, 956 (2012).
- [20] P. Chang, A.E. Broderick, C. Pfrommer, *ApJ* **752**, 23 (2012).
- [21] F. de Gasperin *et al.*, *A&A* **547**, 56 (2012).
- [22] D. Donato, G. Ghisellini, G. Tagliaferri, G. Fossati, *A&A* **375**, 739 (2001).
- [23] E. Dwek, F. Krennrich, *Aph* **43**, 112 (2013).
- [24] G. Ghisellini, L. Maraschi, F. Tavecchio, *MNRAS* **396**, 105 (2009).
- [25] M.J. Hardcastle, C.C. Cheung, I.J. Feain, . Stawarz, *MNRAS* **393**, 1041 (2009).
- [26] J.-P. Lenain *et al.*, *A&A* **524**, 72 (2010).
- [27] M. Loewenstein, E.G. Zweibel, M.C. Begelman, *ApJ* **377**, 392 (1991).
- [28] E. Massaro *et al.*, *A&A* **495**, 691 (2009).
- [29] B.R. McNamara and P.E.J. Nulsen, *NJPh* **14**, 055023 (2012).
- [30] A. Neronov and I. Vovk, *Science* **328**, 73 (2010).
- [31] C. Pfrommer, *subm.* (2013), [arXiv:1303.5443](#).
- [32] C. Pfrommer, P. Chang, A.E. Broderick, *ApJ* **752**, 24 (2012).
- [33] A. Pinzke and C. Pfrommer, *MNRAS* **409**, 449 (2010).
- [34] E. Puchwein, C. Pfrommer, V. Springel, P. Chang, A.E. Broderick, *MNRAS* **423**, 149 (2012).
- [35] F.M. Rieger, F. Aharonian, *Modern Physics Letters A* **27**, 30030 (2012).
- [36] F.M. Rieger, E. de Ona-Wilhelmi, F. Aharonian, [arXiv:1302.5603](#).
- [37] R. Schlickeiser, D. Ibscher, M. Supsar, *ApJ* **758**, 102 (2012).
- [38] A.M. Taylor, I. Vovk, A. Neronov, *A&A* **529**, 144 (2011).
- [39] C.M. Urry and P. Padovani, *PASP* **107**, 803 (1995).